Visualizing spatial and temporal heterogeneity of single molecule rotational diffusion in a glassy polymer by defocused wide-field imaging

Uji-i, Hiroshi; Melnikov, Sergey M.; Deres, Ania; Bergamini, Giacomo; Schryver, Frans De; Herrmann, Andreas; Müllen, Klaus; Enderlein, Jörg; Hofkens, Johan

Published in:
Polymer

Publication date:
2006

Citation for published version (APA):
Uji-i, H., Melnikov, S. M., Deres, A., Bergamini, G., Schryver, F. D., Herrmann, A., ... Hofkens, J. (2006). Visualizing spatial and temporal heterogeneity of single molecule rotational diffusion in a glassy polymer by defocused wide-field imaging. *Polymer*, 47(7), 2511-2518.

ELSEVIER

Visualizing spatial and temporal heterogeneity of single molecule rotational diffusion in a glassy polymer by defocused wide-field imaging

Hiroshi Uji-i [a], Sergey M. Melnikov [a], Ania Deres [a], Giacomo Bergamini [a,d], Frans De Schryver [a], Andreas Herrmann [b], Klaus Müllen [b], Jörg Enderlein [c,**], Johan Hofkens [a,*]

[a] *Department of Chemistry, Katholieke Universiteit Leuven, Celestijnenlaan 200 F, 3001 Heverlee, Belgium*
[b] *Max-Planck-Institut für Polymerforschung, Ackermannweg 10, D-55128 Mainz, Germany*
[c] *Institute for Biological Information Processing I, Forschungszentrum Jülich, D-52425 Jülich, Germany*
[d] *Dipartimento Chim G Ciamician, Università Bologna, Via Selmi 2, Bologna I-40126, Italy*

Abstract

Defocused wide-field fluorescence microscopy was used to follow the 3D molecular rotational diffusion of a fluorescent probe molecule in a polymer thin film. The technique allows for visualizing the molecular reorientation both in-plane and out-of-plane. The local environmental change driven by heterogeneous dynamics of the polymer can be probed on a scale of 1 μm as demonstrated by parallel imaging of several molecules. A multi-component rotational diffusion decay is observed which might reflect both different relaxation regimes of the polymer as well as rapid changes of the local environment.
© 2006 Elsevier Ltd. All rights reserved.

1. Introduction

Over the last 15 years, single molecule spectroscopy (SMS) has been established as a new tool in the ever expanding range of spectroscopic methods. SMS is especially useful to study inhomogeneous systems [1–7]. Biological systems are by their nature highly heterogeneous and as such perfect targets for SMS. From this it is clear that, next to biological samples, polymers form a study object of SMS as polymers are very often heterogeneous in their behavior [5–7]. Many theories that describe polymer properties are based on a microscopic picture [8,9] that now can be evaluated experimentally by applying single molecule techniques. A variety of polymers and several SM techniques have been exploited for these studies [10–19]. Some groups focused their attention on unraveling the complex photophysics of conjugated polymers and tried to establish a relationship between single polymer chain conformation, interaction with the surrounding inert matrix and the observed photophysics [10–13]. Other groups devoted effort in testing and validating, on a microscopic level, the theories developed to describe the physical properties of polymers. Especially the behavior close to the glass transition temperature of the polymer under consideration has drawn a lot of attention. In order to validate theories describing this transition, probe molecules are embedded in the polymer. One approach consists of measuring changes in the radiative lifetime of a single molecule below or close to the glass transition temperature [14,15]. According to the free volume theory, the free volume that can be thought of as sub-nanometer holes caused by structural disorder in the polymer, fluctuates around the probe molecule both in time and in space. This in turn causes changes in the local density around the probe molecule and subsequent changes in the radiative lifetime. Alternatively, segmental relaxation above T_g can be probed by the rotational motion, of a probe molecule, induced by the relaxation process [16–19]. The rotation of single molecules is typically followed by measuring the degree and orientation of linear polarization of fluorescence, resulting from the projection of the emission dipole orientation on a two-dimensional plane. This usually leads to a loss of the out-of-plane information of the molecule under investigation.

However, several detection schemes were developed for measuring the 3D orientation of single molecules via

the orientation of their transition dipole moment [20–30]. Scanning near field optical microscopy [21,22] as well as confocal microscopy, eventually modified by using annular beams [23,24], have been used for this goal. Also, fluorescence wide-field microscopy has been applied to get information about the angular distribution of single molecule's fluorescence emission (and hence 3D orientation) by defined image defocusing [25,26,29] or by introducing aberrations [27]. The latter approach was used by Dickson and co-workers in their study of polymer (poly(methyl methacrylate)) below T_g. Here we use defocused wide-field imaging in combination with an extremely robust perylendiimide dye (Fig. 1) to study rotational motion of the dye in a polymer with a T_g close to room temperature. Defocused imaging offers several advantages: it allows for highly parallel data collection by looking at many molecules in the field of view and it gives exact information on the 3D orientation as mentioned before [25,26]. Furthermore the photostability of the dye used allows imaging for an extended period of time (more than 30 min). In this way, spatial and temporal inhomogeneities of the rotational movement of the dyes could be demonstrated. The high quality of the images allows for a decomposition of the movement in the x–y plane and the z-plane. We could demonstrate both static and temporal heterogeneity in polymer relaxation, in good agreement with previous literature reports. Furthermore, the full 3D rotational diffusion can be analyzed using a model for an isotropic rotor. The detailed analysis

suggests the existence of different relaxation regimes for the polymer used.

2. Experimental

2.1. Defocused imaging and analysis

Defocused imaging of a single molecule was performed using a wide-field fluorescent microscope consisting of an inverted optical microscope (IX71, Olympus) equipped with 1.3-N.A., 100× oil immersion objective (Plan Fluorite, Olympus) and a highly sensitive cooled CCD camera with 512×512 pixels (cascade 512B, Princeton Instruments Inc.) with a pixel size of 16×16 μm^2. For excitation, the 532 nm light from a diode-pumped solid state laser (CDPS532M-50, JDS Uniphase Co.) was used. The wide-field illumination for excitation was achieved by focusing the expanded and collimated laser beam onto the back-focal plane of the objective (Köhler illumination mode). The polarization of excitation light in the sample plane was carefully tuned to be circular using zero-order $\lambda/4$ and $\lambda/2$ waveplates in order to compensate for polarization shift of the dichroic mirror. The power density in the plane was usually adjusted to 1–10 kW/cm^2. Emission is collected by the same objective and imaged by the CCD after passing through a dichroic mirror (z532rdc, Chroma Technology Co.) and an additional spectral filter (HQ542LP, Chroma Technology Co.) removing the excitation light. The image was further magnified 3.3 times with a camera lens before the CCD camera, resulting in a maximum field of view of 24.6×24.6 μm^2 (48×48 nm^2 per pixel). The imaging was performed under N$_2$ atmosphere to reduce the effect of photobleaching. All measurements were done at 295±2 K.

By taking defocused images, the angular distribution of the emitted fluorescence of a single molecule is mapped as a spatial distribution of intensity, which reflects 3D molecular orientation [25,26]. To obtain the images, the sample was positioned by ~1 μm toward the microscope objective from the focus using a piezoelectric transducer (PI5173Cl, Physik Instrumente). Integration times per frame vary between 200 ms and 1 s, depending on the excitation power used. The obtained defocused images were analyzed using a routine written in MatLab software, in order to determine molecular orientation in each image frame. The images were first analyzed using a pattern matching routine to determine roughly the molecular orientation in each image frame [25,26], and then fitted precisely by a non-linear least-square algorithm, which determines the molecular dipole orientation and its position coordinate with an accuracy limited by the finite signal-to-noise ratio of experimentally measured images. The images were filtered for high-frequent noise by a low-pass filter to improve accuracy of the fitting.

2.2. Sample preparation

Thin polymer films (thickness of 50–100 nm) were prepared on cleaned glass cover slips by spincoating from 0.5 to 1.0 wt% solution of poly(methyl acrylate) (PMA, bulk T_g~281 K,

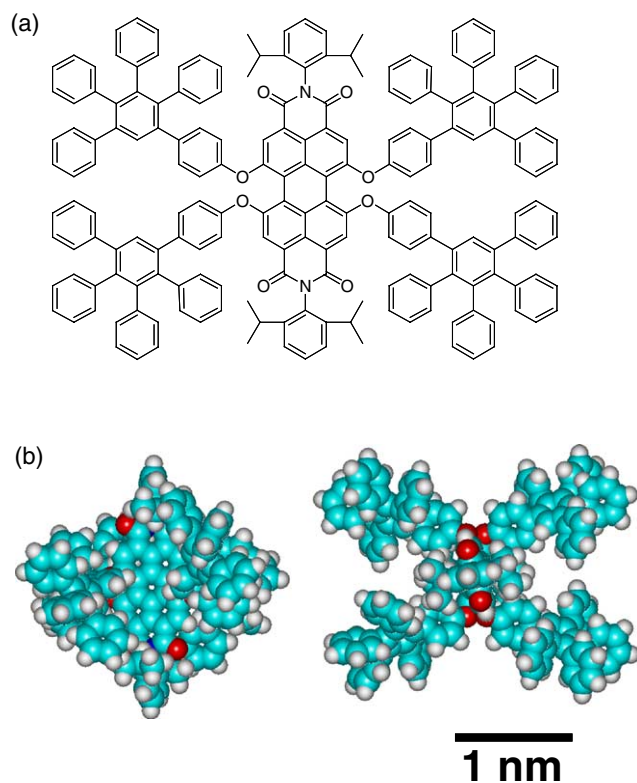Fig. 1. (a) The chemical structure of compound **1**. (b) 3D representation of **1** from different view points; along the vertical axis of the plane of the perylenediimide core (left) and along the long axis of the perylenediimide core (right).

$M_n = 11,340$ g/mol, $M_w/M_n = 3.65$, purchased from Aldrich and used without further purifications) containing 1–10 nM of a perylene diimide substituted with polyphenylene groups in the bay positions (compound **1**, $M_w = 2601.25$, see the structure in Fig. 1) in toluene. The number-average molecular weight (M_w) and polydispersity index (M_w/M_n) was estimated using size exclusion chromatography (SCL-10Avp, Shimazu Co.). The films were put in vacuum at room temperature for more than 2 h in order to remove residual solvent. All samples were kept in vacuum before the experiment and measured within 1 day after preparation. Note that the glass transition temperature of a thin film can be lower than the glass transition temperature measured in bulk [31].

3. Results and discussion

Fig. 2 shows a typical defocused image of **1** embedded in a thin PMA film at an excitation power of 1 kW/cm^2 with 1 s integration. Although various emission patterns are observed, the majority of spots show a clear two-lobe pattern. As can be seen in the picture, 25% of the molecules show a substantial out-of-plane contribution (molecules indicated by the dashed white circles). The fluorescence intensity varies from molecule to molecule. Especially molecules oriented out-of-plane are not excited efficiently [28] and, therefore, show lower emission intensity. The center position of the defocused pattern corresponds to the spatial coordinate of the corresponding single molecule, and can be determined by the image analysis. No translational mobility could be observed. The center part of the defocused pattern (the bright two-lobe) is imaged with 22×22 pixels so that the pattern of a single molecule occupies an area of about 1×1 μm^2 on the image. Thus, molecules separated by this distance can be analyzed by our analytical method. For precise analysis of the out-of-plane orientation,
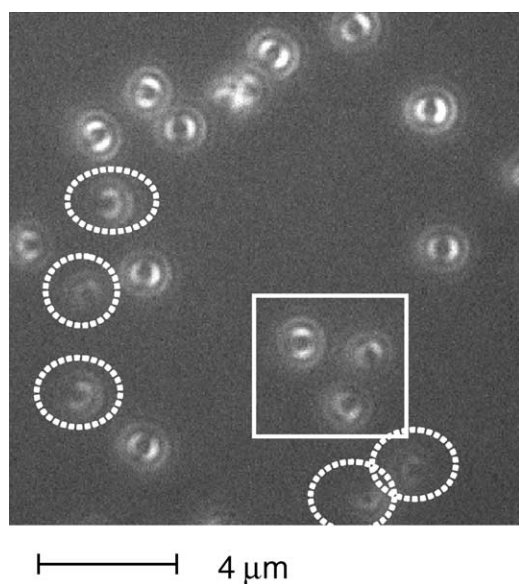
the ideal separation between molecules is 1.5 μm, because the outer rim of the pattern is very helpful for the analysis (see below).

Fig. 3 shows examples of calculated emission patterns for different out-of-plane orientations (θ) of the transition dipole moment of a single molecule (defocusing depth 1 μm, for details on the calculations see [25,26]). The in-plane orientation of the transition dipole moment was kept constant during the calculation. In order to demonstrate the changes in calculated patterns for different out-of-plane orientations, the patterns are calculated for changes in θ of 10°. Clearly the bilaterally symmetric two-lobe pattern at 90° (completely in-plane orientation) changes into asymmetric ringed pattern as the out-of-plane angle (θ) decreases. At 0° (complete out-of-plane), the pattern has a symmetric circular ring shape. The size of the inner lobe part and the symmetry of the outer rim are crucial in addition to the shape for the analysis. The size of lobe is very sensitive to the out-of-plane angle. The symmetry of the rim is often helpful to determine the in-plane angle, especially for images with a low signal-to-noise ratio. Note that it becomes progressively harder to distinguish patterns with an out-of-plane angle of less than 50°.

The sequence shown in Fig. 4(a) consists of snapshots of an individual molecule showing rotational diffusion in a PMA film as function of time. An image is shown every 1.4 s (with 1 s integration and 0.4 s interval time). The sequence A represents experimental data, the sequence B

Fig. 2. A typical defocused image of **1** embedded in a 50 nm film of PMA with 1 μm defocusing toward the sample. The white dashed circles indicate molecules, which are substantially oriented out-of-plane. The white square are the molecules discussed in Figs. 5–7.
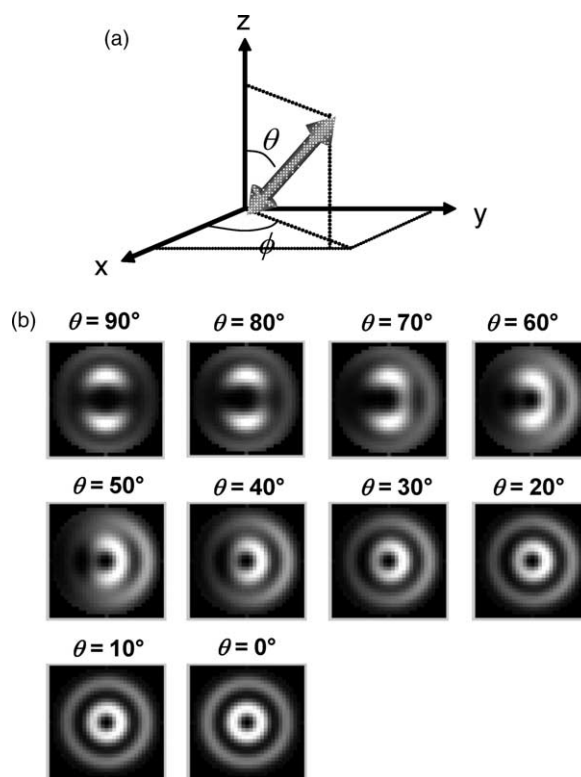

Fig. 3. Calculated defocused patterns of a single molecule for 10 different out-of-plane orientations. These values of θ are the same as those used in pre-analysis using the pattern-matching.
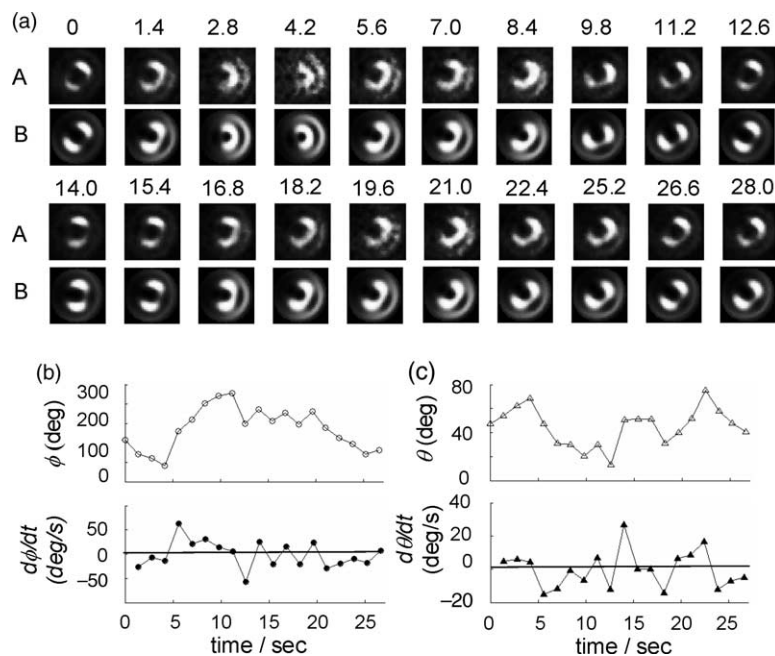
Fig. 4. (a) Snapshots of experimentally observed emission patterns (sequence A) and corresponding computed patterns (sequence B) as a function of time. Transition dipole orientation trajectories and their first time derivatives are shown for the in-plane (b) and out-of-plane component (c), respectively.

shows the corresponding calculated patterns. By fitting each emission pattern as function of time, transition dipole orientation trajectories are obtained (Fig. 4(b)). The first derivative of such trajectory clearly shows that the rotational diffusion is not unidirectional but random instead. This is to be expected since the dynamics of the probe molecule are driven by polymer segmental motions and hence result from relaxations of the polymer chains, which should be random.

Fig. 5(a) shows three molecules that are relatively close to each other in space. Fig. 5(b)–(d) shows the projection maps for molecules **1**–**3** shown in Fig. 5(a), respectively. The defocused images were obtained with 1 s integration and 0.4 s interval time. Two different types of behavior can be observed in the maps. Molecule **2** (Fig. 5(c)) exhibits fast rotations with no preference for any orientation. On the other hand, molecules **1** and **3** are temporarily locked in one orientation and occasionally jumps to a completely different orientation occur. For example, molecule **1** is first oriented in the region indicated by the black line but undergoes a jump in orientation, indicated by the red line, after 970 s. Molecule **3** shows an even more complex behavior: though it is locked in three different orientations for 1760 s, it starts rotating in rather wide range of angles afterwards. From that point on, completely different rotational dynamics are observed. This clearly reflects temporal heterogeneity of polymer relaxations. Most interestingly, molecule **3** passes through the initial region on the projection map, observed between 0 and 190 s and indicated in black, when jumping from the green region into the red region after 890 s. These results clearly indicate temporal heterogeneity and may point to a memory effect in polymer relaxation at the dimension of the probe molecule, meaning approximately 3 nm.

A more quantitative evaluation of the phenomena seen in the projection maps can be obtained by constructing time trajectories of the dipole orientation and analyzing the observed fluctuations by correlation functions. Fig. 6 shows the time trajectories of the dipole orientation and their first derivatives for the three molecules in Fig. 5(a). Several important observations can be made for these molecules. First, the analysis of the rotational movement of these molecules clearly indicates spatial heterogeneity on a micrometer scale (Fig. 5(a) and video 1 in Supporting information). Secondly, molecule **1** (Fig. 6(a)) shows no large changes in rotation rate during the observation time of 2500 s. The behavior of molecule **2** (Fig. 6(b)) is in striking contrast with the behavior of molecule **1**. Clear changes in the rotational rate can be observed, both for the in- and the out-of-plane part of the rotation. This difference between these molecules is also reflected in the correlation function of the rotational movement (vide infra). Molecule **3** (Fig. 6(c)) shows a wide variety of behaviors. Changes of the rotation rate for both in- and out-of-plane rotation components occur after 1800 s. These changes correspond to the wide angular distribution observed in the projection map in Fig. 5 after 1800 s, indicated in blue. Note that for the kind of polymer matrix used, temporal heterogeneity is expected on a time scale of about 500 s at room temperature [18].

In order to evaluate our experimental technique and in order to compare the results obtained with data reported earlier in literature, we first estimate the in-plane component of the rotational diffusion using a similar analysis as reported in [18]. The autocorrelation function was calculated using

$$C(t) = \frac{\langle A(t')A(t'+t)\rangle}{\langle A(t')A(t')\rangle} \qquad (1)$$
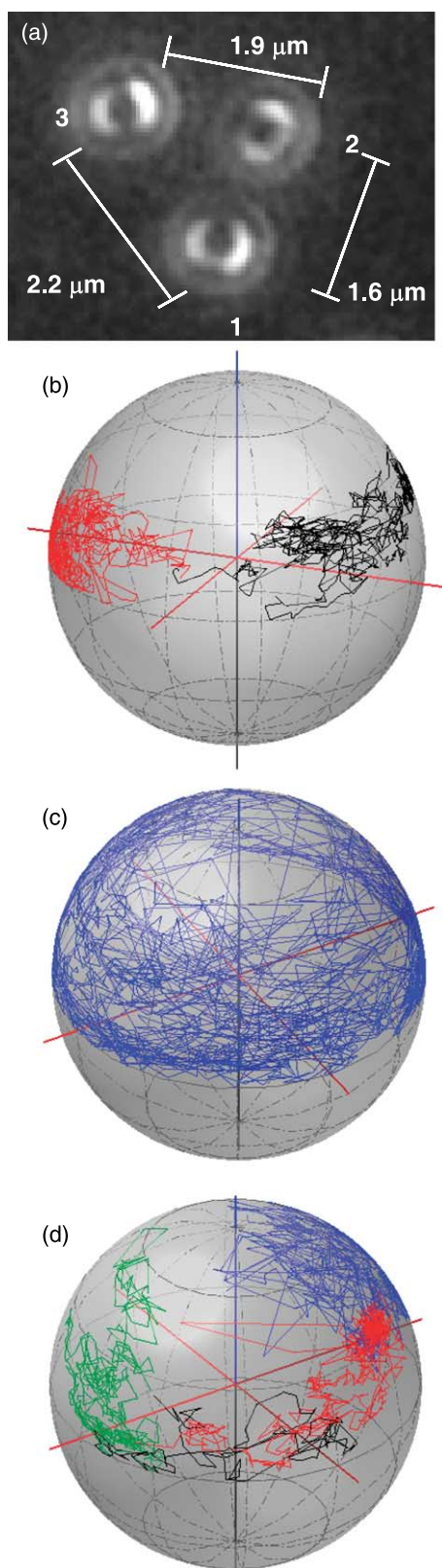
Fig. 5. Spatial and temporal heterogeneity of dynamics at 295 K. (a) A zoom of the three molecules indicated by the white square in Fig. 2. Molecules are separated by $\sim$1.5 μm. (b)–(d) Projection maps for molecule **1**–**3**, respectively. The red lines indicate the *x*–*y* image plane and blue line is the optical (*z*) axis: 0–960 s (black) and 960–2380 s (red) in (b), 0–190 s (black), 190–895 s (green), 895–1763 s (red), and 1763–2940 (blue) in (d).

where $A(t) = \cos(2\phi(t))$. The decay of $C(t)$ is then fitted with Kohlrausch–Williams–Watt (KWW) stretched exponential function:

$$C(t) = \sum_i \exp\left[-\left(\frac{t}{\tau_{i\ \text{KWW}}}\right)^{\beta_{i\ \text{KWW}}}\right] \qquad (2)$$

The averaged time scale of rotational diffusion (τ_c) is estimated by $\tau_\text{c} = \int_0^\infty C(t)\mathrm{d}t$. The correlation functions and the fitting results of the three molecules in Fig. 5(a) are illustrated in Fig. 7. The individual molecules show significantly different behavior. The correlation function of molecule **1** and **3** can be fitted with a stretched exponential decay with a β_KWW close to one. The τ_c was estimated to be 164 and 230 s for molecule **1** and **3**, respectively. These values are more than twice slower than the correlation times of rhodamine 6G and rubrene embedded in PMA in the earlier reports [18,32]. This is not surprising since it is known that rotation of large probes is more hindered and can deviate from the collective relaxation of surrounding matrix, resulting in high-β_KWW value and large τ_KWW [32]. On the other hand, molecule **2** shows a much faster average decay of $\tau_\text{c} = 47$ s actually consisting of two components, yielding $\tau_{1\ \text{KBB}} = 4.2$ s ($\beta_{1\ \text{KBB}} = 1.0$) and $\tau_{2\ \text{KBB}} = 44$ s ($\beta_{2\ \text{KBB}} = 0.7$). This smaller value of $\tau_{2\ \text{KBB}}$ can be related to spatially heterogeneous dynamics present in polymers, especially in the very poly-disperse PMA matrix used. However, interfacial effects at the air/polymer or polymer/glass interfaces where the probe molecule might exhibit different dynamics cannot be excluded. The $\tau_{1\ \text{KBB}}$ might represent a shorter second relaxation regime of the polymer. Note that the mismatch between the correlation function and the exponential at the initial part of molecule **1** might also indicate the presence of this faster polymer relaxation regime. However, it was recently argued that for the approach described above, e.g. analyzing a 3D rotation by only considering the in-plane contribution by calculating the linear dichroism, even an isotropic rotational diffusion can lead to non-exponential correlation functions [33]. If so, the obtained stretched exponential behavior of the correlation functions might be the result of a complex mixture of an analysis artifact and polymer dynamics. Indeed, assume one is interested in the probability that the dipole orientation, within time t, changes its polar angle from θ_0 to θ_1, and its in-plane angle by ϕ, as shown in the Fig. 8.

For an isotropic rotator, the associated probability distribution is given by:

$$P(\theta, \phi, t|\theta_0) = \sum_{n=0}^{\infty} \sum_{m=-n}^{n} \frac{2n+1}{4\pi} \frac{(n-|m|)!}{(n+|m|)!}$$
$$P_n^m(\cos\theta)P_n^m(\cos\theta_0)\exp[im\phi - n(n+1)D_\text{rot}t] \qquad (3)$$

where P_n^m are associated Legendre polynomials. D_rot is the rotational diffusion constant. Knowing this distribution, one
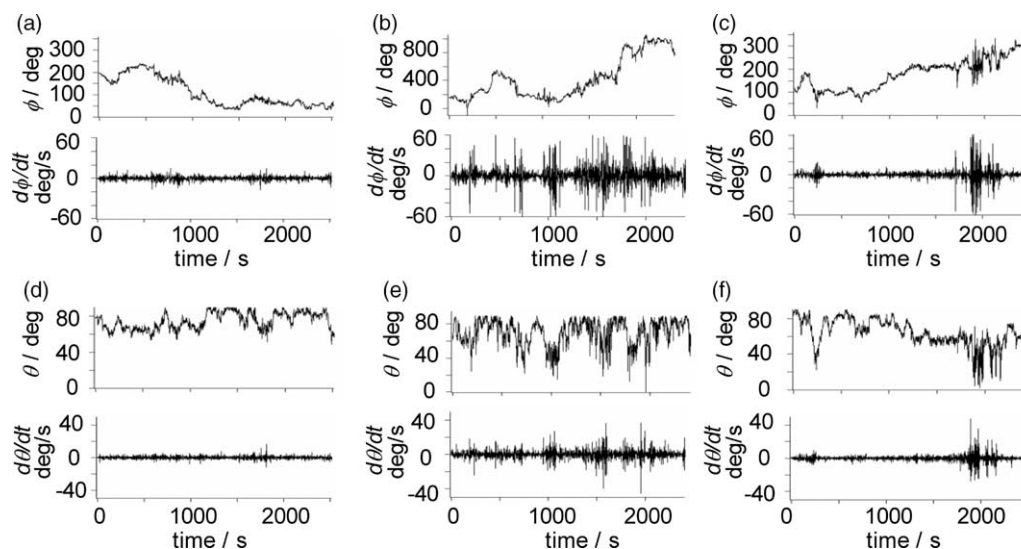
Fig. 6. Transition dipole orientation trajectories in-plane and out-of-plane and their time derivatives for molecule **1** (a) and (d), **2** (b) and (e), and **3** (c) and (f).

can compute the average of the cos 2ϕ as

$$
\begin{aligned}
\langle \cos 2\phi \rangle &= \int_0^\pi d\theta \sin \theta \int_0^\pi d\theta_0 \sin \theta_0 \int_0^{2\pi} d\phi P(\theta, \phi, t|\theta_0) \cos 2\phi \\
&= \int_0^\pi d\theta \sin \theta \int_0^\pi d\theta_0 \sin \theta_0 \sum_{n=2}^\infty \frac{2n+1}{2} \frac{(n-2)!}{(n+2)!} \\
&\quad \times P_n^2(\cos \theta) P_n^2(\cos \theta_0) \exp[-n(n+1)D_{\text{rot}}t] \\
&= 8 \sum_{n=1}^\infty (4n+1) \frac{(2n-2)!}{(2n+2)!} \exp[-2n(2n+1)D_{\text{rot}}t]
\end{aligned}
$$

$$(4)$$

which is a complicated infinite series of exponential decays. As stated above, it is difficult to interpret the physical meaning.

A very recent report claims, however, that the above mentioned effect is minimal when one uses high NA objective lenses [34]. The authors state that to best compare to ensemble measurements of reorientation dynamics it would be ideal to measure the full three-dimensional orientation of the molecule. They also mention that single molecule techniques able of measuring the 3D orientation require many photons to determine the orientation and thus limit the length of trajectories and impair useful correlation analysis. Here, we demonstrate measurements of long trajectories of the full 3D orientation with high signal-to-noise ratio that allow correlation analysis.

The 3D rotational diffusion equation for an isotropic rotational diffusion with diffusion constant D_{rot} on the other hand is simply is given by

$$
\frac{\partial h(\Psi, t)}{\partial t} = D_{\text{rot}} \frac{1}{\sin \Psi} \frac{\partial}{\partial \Psi} \sin \Psi \frac{\partial h(\Psi, t)}{\partial \Psi}
$$

$$(5)$$

where $h(\Psi, t)$ is the orientation distribution function. Ψ is angular change as defined by $\Psi = \arccos(\mathbf{n}_t \cdot \mathbf{n}_{t+\delta t})$, where $\mathbf{n}_t$ is the unit orientation vector of the molecular dipole moments at

time t. The average of $\langle \cos(\Psi) \rangle$ over Ψ as function of time,

$$
\langle \cos(\Psi) \rangle = \int_0^\pi d(\Psi) \sin(\Psi) h(\Psi, t) \cos(\Psi) = \exp(-2D_{\text{rot}}t)
$$

$$(6)$$

shows a single exponential decay. The relaxation time is given by $\tau = 1/2D_{\text{rot}}$

We analyzed 54 of the molecules shown in Fig. 9 using the mathematics for a 3D isotropic rotor as outlined above (Eqs. (5)
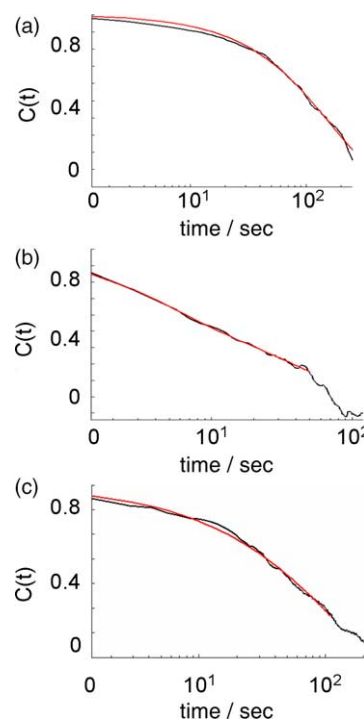

Fig. 7. Correlation function of the in-plane transition dipole orientation of molecule **1** (a) ($\tau_c = 164$ s, $\tau_{\text{KBB}} = 160$ s, $\beta_{\text{KBB}} = 0.95$), **2** (b) ($\tau_c = 47$ s, $\tau_{1\,\text{KBB}} = 4.2$ s, $\beta_{1\,\text{KBB}} = 1.0$ and $\tau_{2\,\text{KBB}} = 49$ s, $\beta_{2\,\text{KBB}} = 0.65$), and **3** (c) ($\tau_c = 231$ s, $\tau_{\text{KBB}} = 169$ s, $\beta_{\text{KBB}} = 0.65$).
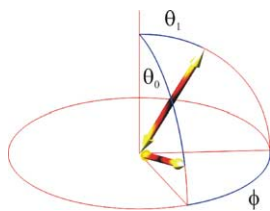
Fig. 8. Schematic representation of the angular changes in a time interval t for a 3D rotational diffusion of the transition dipole. The in-plane projection of the transition dipole is also shown.

and (6)). The images were taken with 200 ms integration time and no interval time between the different frames. Although in this contribution trajectories are analyzed with 1000 data points (200 ms integration time per image) to demonstrate the method, it is possible to obtain trajectories with more than 10,000 data points if one uses integration times of 50 ms. Note that the image in Fig. 9 a sample film of more than 100 nm was used to rule out the earlier discussed interfacial effects.

Fig. 10(a) shows typical decays and fitting results. Again, two different time scales were found in the correlation functions. The best fitting could be obtained by using bi-exponential decays. The obtained values of the diffusion coefficients for 40 of the 54 molecules, showing a clear bi-exponential decay, are shown in Fig. 10(b). Note that the difference between the fast and the slow rotational component is nearly two orders of magnitude. The fast component of most molecules is distributed between 0.1 and 10 s and the slow decay between several hundreds to thousands of seconds. From a phenomenological point of view, it is well know that fast local rearrangements of a polymer (referred as Johari–Goldstein β process, or secondary relaxation) are followed by the main slower relaxation, commonly termed as α process. This process involves cooperative molecular motions. The observed relaxation time scale may reflect different relaxation regimes of polymer relaxation dynamics. Namely, the observed fast relaxation of molecular rotation might reflect the β-process polymer relaxation and the slower rotational diffusion could reflect the collective polymer motion. The tentative assignment made here to different relaxation regimes will be further investigated in detail by using a variety of fluorescent probes

Fig. 10. (a) Typical autocorrelation functions ($\bigcirc$) and bi-exponential fits (solid line) for four molecules from Fig. 9. (b) The distribution of diffusion coefficients for 40 of the molecules in Fig. 9.

with different sizes and aspect ratios in well-defined mono-disperse polymer matrixes.

4. Conclusions

We demonstrated the potential of defocused wide-field fluorescence microscopy to monitor molecular rotational diffusion in a glassy polymer. Due to the good signal-to-noise ratio of the fluorescence images, 3D reorientation of molecular dipole moment could be followed. Using the full 3D rotation avoids the introduction of analysis artifacts. The data clearly evidence non-directional molecular rotation, resulting from random polymer relaxation. We showed that the autocorrelation function for the rotation of different probe molecules can vary greatly, resulting in large differences in rotational correlation times. This is due to the highly poly-disperse PMA matrix used. The advantage of wide-field imaging (parallel data collection of many molecules) allows us to prove spatially heterogeneous dynamics on the sub-1 μm scale, which is a promising result for investigating local environmental changes in phase separation processes or for investigating changes in viscosity during polymerization reactions. The 3D rotational correlation function could only be fitted bi-exponential. This might relate to different relaxation regimes predicted by polymer theories. In order to evaluate this hypothesis, experiments in better-defined, mono-disperse polymers will be conducted.
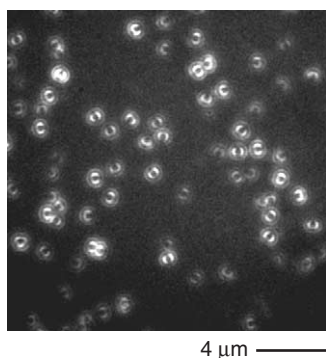

Fig. 9. A defocused image used for the statistical analysis of 54 of the molecules in view. The images were taken with 200 ms integration and no interval time between frames.
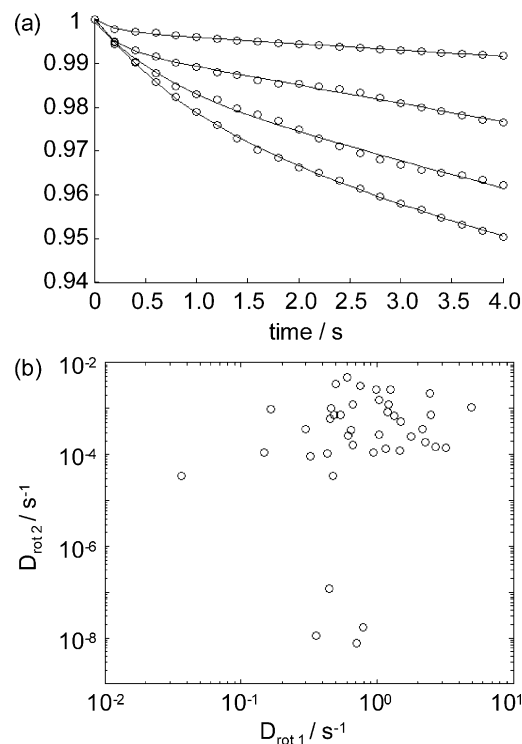
Acknowledgements

Supplementary data

Supplementary data associated with this article can be found at doi:10.1016/j.polymer.2005.11.094

References

[1] Ambrose WP, Goodwin PM, Jett JH, Van Orden A, Werner JH, Keller RA. Chem Rev 1999;99:2929–56.

[2] Moerner WE, Fromm DP. Rev Sci Instrum 2003;78:3597–619.

[3] Kulzer F, Orrit M. Annu Rev Phys Chem 2004;55:585–611.

[4] Enderlein J, Böhmer M. Chem Phys Chem 2003;4:792–808.

[5] Smith DE, Perkins TT, Chu S. Phys Rev Lett 1995;75:4146–9.

[6] Chu S. Philos Trans R Soc London, A 2003;361:689–98.

[7] Smith DE, Babcock HP, Chu S. Science 1999;283:1724–7.

[8] Schilling R. In: Randons G, Just W, Haeussler P, editors. Collective dynamics of nonlinear and disordered systems. Berlin: Springer; 2003 [and references therein].

[9] Götze W. J Phys 1999;11:A1–A45 [and references therein].

[10] Barbara PF, Gesquiere AJ, Park SJ, Young JL. Acc Chem Res 2005;38: 602–10.

[11] Sartori SS, De Feyter S, Hofkens J, Van der Auweraer M, De Schryver FC, Brunner K, et al. Macromolecules 2003;36:500–7.

[12] Schindler F, Lupton JM, Feldmann J, Schef U. Proc Natl Acad USA 2004; 101:14695–14700.

[13] Huser T, Yan M, Rothberg LJ. Proc Natl Acad Sci USA 2000;97: 11187–91.

[14] (a) Vallee RAL, Tomczak N, Kuipers L, Vancso GJ, van Hulst NF. Phys Rev Lett 2003;91(3):038301.

(b) Vallee RAL, Marsal P, Braeken E, Habuchi S, De Schryver FC, Van der Auweraer M, et al. J Am Chem Soc 2005;127(34):12011–20.

(c) Vallee RAL, Cotlet M, Hofkens J, De Schryver FC, Müllen K. Macromolecules 2003;36(20):7752–8.

[15] Biju VP, Ye JY, Ishikawa M. J Phys Chem B 2003;107:10729–35.

[16] Ha T, Laurence TA, Chemla DS, Weiss S. J Phys Chem B 1999;103: 6839–50.

[17] Tomczak N, Vallée RAL, van Dijk EMHP, García-Parajó M, Kuipers L, van Hulst NF, et al. Eur Polym J 2004;40:1001–11.

[18] (a) Deschenes LA, Vanden Bout DA. J Phys Chem B 2001;105: 11978–85.

(b) Deschenes LA, Vanden Bout DA. Science 2001;292:255–8.

(c) Deschenes LA, Vanden Bout DA. J Chem Phys 2002;116:5850–6.

[19] Zhou Q. J Korean Phys Soc 2005;47:S190–S3.

[20] Prummer M, Sick B, Hecht B, Wild UP. J Chem Phys 2003;118: 9824–9.

[21] Veerman JA, Garcia-Parajo MF, Kuipers L, van Hulst NF. J Microsc 1999;194:477–82.

[22] Moerland RJ, van Hulst NF. Opt Express 2005;13:1604–14.

[23] Sick B, Hecht B, Novotny L. Phys Rev Lett 2000;85:4482–5.

[24] Novoty J, Beversluis MR, Youngworth KS, Brown TG. Phys Rev Lett 2001;86:5251–4.

[25] Schroeyers W, Vallee RAL, Patra D, Hofkens J, Habuchi S, Vosch T, et al. J Am Chem Soc 2004;126(44):14310–1.

[26] (a) Böhmer M, Enderlein J. J Opt Soc Am B 2003;20:554–9.

(b) Patra D, Gregor I, Enderlein J. J Phys Chem A 2004;108:6836–41.

[27] Bartko AP, Xu K, Dickson RM. Phys Rev Lett 2002;89:026101.

[28] Piwonski H, Stupperich C, Hartschuh A, Sepiol J, Meixner A, Waluk J. J Am Chem Soc 2005;127:5302–3.

[29] (a) Jasny J, Sepiol J. Chem Phys Lett 1997;273(5–6):439–43.

(b) Sepiol J, Jasny J, Keller J, Wild UP. Chem Phys Lett 1997;273(5–6): 444–8.

[30] Fourkas JT. Opt Lett 2001;26:211–3.

[31] Roth CB, Dutcher JR. J Electroanal Chem 2005;584:13–22.

[32] Inoue T, Cicerone MT, Ediger MD. Macromolecules 1995;28:3425–33.

[33] Hinze G, Diezemann G, Basche Th. Phys Rev Lett 2004;23(20): 203001.

[34] Wei CYJ, Kim YH, Darst RK, Rossky PJ, Vanden Bout DA. Phys Rev Lett 2005;95(17):173001.